Wall velocity gradients in Taylor-Couette-Poiseuille flow

Vaclav Sobolik, Magdalena Kristiawan, Alioune El Faye

Wall velocity gradients in Taylor-Couette-Poiseuille flow

Vaclav Sobolik, [1] Magdalena Kristiawan, Alioune Faye

University of La Rochelle, UFR Sciences, LASIE
Av. Michel Crepeau, 17042 La Rochelle, France
[1] INRA BIA Biopolymères, Interactions Assemblages
Rue de la Géraudière, 44316 NANTES, France
E-mail: vsobolik@univ-lr.fr

Keywords: Vortices, electrodiffusion method, three-segment probes

Abstract

Experiments were carried out in the flow between concentric cylinders with the inner cylinder rotating and outer cylinder fixed. The radius and aspect ratios were 0.8 and 44, respectively. The electrodiffusion method with a three-segment and simple micro-electrodes was used for study of the axial and azimuthal components of velocity gradient at the outer cylinder. The axial distributions of the components of wall velocity gradient were obtained by sweeping the vortices along the probes using axial flow. The wavelength and phase celerity of waves, height of vortices and their drifting velocity were calculated from the measured limiting diffusion currents.

I. Introduction

Several techniques can be used for the measurements of velocity gradients at the solid-liquid interface. Using dissolution of substances like benzoic acid (Gogoi and Dutta 1996) or copper (Gruber and Melin 2003, Raguin et al. 2001) the time mean values can be estimated. A little more information can provide visualisations by dye chemisorption at polymers (Kuhnel and Kottke 1998). The measurement of the current of an electrochemical reaction, i.e. the electrodiffusion (polarographic) method (Cognet 1971, Lebouché 1970), is the only method able to follow the space distribution and time evolution of wall velocity gradients. This method is based on the measurement of the electric current limited by the transfert of actives species to the working electrode. Using a redox reaction, repetitive measurements can be carried out with a system which does not require addition of active compounds as in the case of the above mentioned method. The measurements are confined to the diffusion boundary layer which is very thin (several micrometers) in the electrolyte solutions (high Schmidt number). This fact distinguishes the electrodiffusion method from the other methods like laser Doppler anemometry, hot film anemometry and particle image velocimetry.

The three-segment probes (see Fig. 1) are composed of three insulated circular sectors that act as working electrodes (Sobolik et al. 1988). For the evaluation of flow direction, we make use of the non-linear dependence of the limiting current density on the distance from the forward electrode edge, $i(x) \sim x^{-1/3}$ (Lévêque 1928). The forward sector has higher current than the sector that lies in his shade. Hence, velocity gradient and its components can be calculated from the limiting diffusion currents passing through the three segments (Wein and Sobolik 1987).

In this work, the electrodiffusion method with a three-segment and simple micro-electrodes was used for the study of the axial (γ_z) and azimuthal (γ_θ) components of velocity gradient at the outer wall of Taylor-Couette flow.

Nomenclature

A	: Amplitude of vortices (s^{-1})
a	: Amplitude of azimuthal waves (s^{-1})
d	: Entrefer between cylinders (m)
h	: Vortex height (m)
I	: Electric current (A)
i	: Density of electric current ($A.m^{-2}$)
n	: Number of azimuthal waves
L	: Distance between electrodes (m)
R_1	: Radius of inner cylinder (m)
R_{ij}	: Correlation coefficient (-)
Ta	: Taylor number = $\Omega R_1^{1/2} d^{3/2}/\mu$ (-)
t	: Time, time lag (s)
v	: Velocity ($m.s^{-1}$)
x	: Distance from the forward electrode edge
z	: Axial co-ordinate (m)
Greek letters	
ϕ	: Flow angle (deg)
γ_k	: Velocity gradient = dv_k/dr (s^{-1})
μ	: Viscosity ($Pa.s$)
Ω	: Rotational rate of inner cylinder ($rad.s^{-1}$)
τ_{ij}	: Shear stress (Pa)
Subscripts	
d	: Vortex
f	: Averaged over azimuthal wave
max	: Maximum
min	: Minimum
θ	: Azimuthal
r	: Radial
tr	: Transition to Taylor vortex flow
w	: Azimuthal wave
z	: Axial
$1,2,3$	: Segments of three-segment probe
$4,5,6$	: Simple electrodes

II. Experimental Facility

Experiments were carried out in the flow between concentric cylinders with the inner cylinder rotating and outer cylinder fixed. The inner cylinder was driven by a stepper motor with electronically controlled rotation rate. The diameters of the outer and inner cylinders were equal to 62 and 49.6 mm, respectively. This corresponds to the radius ratio, R_1/R_2 = 0.8. The aspect ratio was about 44. For simultaneous observation of flow pattern and measurement of velocity gradient and vortex characteristics a Kalliroscope solution was added to the electrolyte.

Several flow regimes were found when axial flow was superposed on rotation of the inner cylinder. Using three-segment probe, see Fig. 1, complete maps of axial and azimuthal components of velocity gradient and their fluctuations at the wall of the outer cylinder were obtained as a function of axial co-ordinate and time. The vortex size (height) and the number and celerity of azimuthal waves were measured by an array of simple electrodes mounted in the wall of the outer cylinder. The arrangement of the electrodiffusion probes along the perimeter of the outer cylinder is shown in Fig. 2. The azimuthal (γ_θ) and axial (γ_z) components of the velocity gradient (γ) were measured by the three-segment probe *3s* with a diameter of 0.5 mm. Simple probes *e4*, *e5* and *e6* were formed by circular electrodes with the same diameter (0.5 mm). The celerity of azimuthal waves was calculated from the time lag (correlation) of currents delivered by *e4* and *e5*. The wave period was obtained from autocorrelation of the current through the electrode *e4*. The wavelength was calculated from wave period and celerity. The vortices were driven by a slow axial flow (*z*-direction) along the probes. The drifting vortex velocity was calculated from the time necessary for a vortex to cover the distance between *e5* and *e6*. The height of vortices was obtained from their period and drifting velocity. The correlations and fast Fourier transformation of measured currents were calculated using Scilab software.

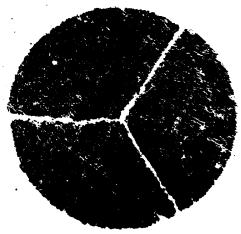

Fig. 1: Three-segment probe with a diameter of 0.5 mm.

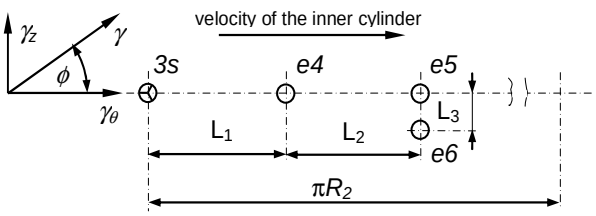

Fig. 2: Arrangement of the three-segment probe *3s* and simple electrodes *e4*, *e5* and *e6* along the perimeter of the outer cylinder.

III. Results and discussions

The limiting diffusion current histories measured by the three-segment probe (I_1, I_2, I_3) and three simple probes (I_4, I_5, I_6) at *Ta*=323 are shown in Fig. 3. The measurements were taken over about one and half vortex pairs with a sampling frequency of 40 1/s. The vortex drifting velocity was 0.14 mm/s. Knowing the drifting velocity, the time axis can be transformed to the axial coordinate *z*. The time t_{d55} corresponds to the passage of a vortex pair along the probe *e5* in axial direction, whereas the time t_{d56} indicates the passage

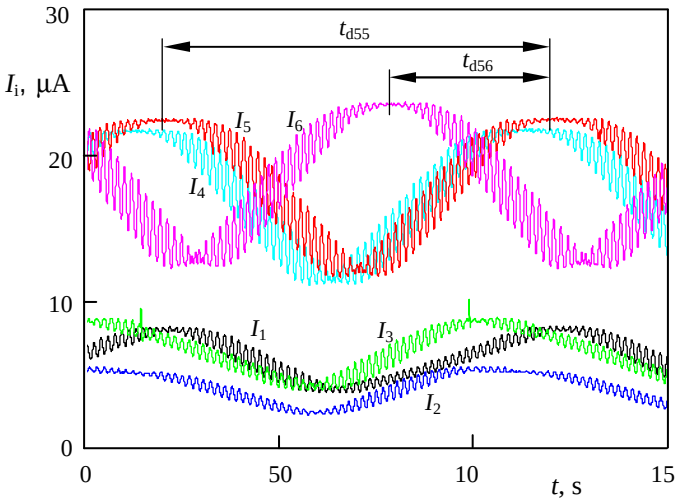

Fig. 3: Current histories: I_1, I_2, I_3 – three-segment probe; I_4, I_5, I_6 – simple electrodes; *Ta* =323

of vortex crest between the probes *e5* and *e6*. The time t_{d56} was used for calculation of vortex drifting velocity and t_{d55} for calculation of vortex height. The azimuthal waves manifest themselves in the signal oscillations. These waves were studied by means of the current correlations R_{4i}, calculated with respect to I_4. The time lag t_{w45} between the autocorrelation of R_{44} and correlation R_{45} (see Fig. 4) corresponds to the passage of a selected wave point between *e4* and *e5*, and t_{w44} to the passage of one wave past *e4*. The time

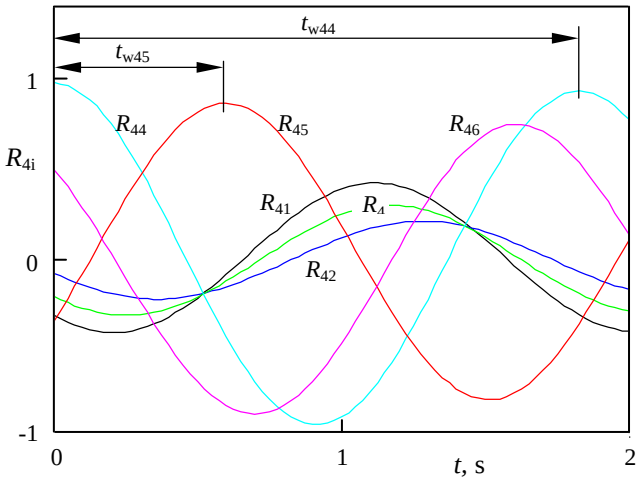

Fig. 4: Correlations with respect to the current I_4

t_{w45} was used for the calculation of azimuthal wave celerity and the wave period t_{w44} for calculation of wavelength. The number of azimuthal waves was obtained by dividing the perimeter of the outer cylinder by the wavelength. The velocity gradient components calculated from currents I_1, I_2, I_3 are shown in Fig. 5a. The z-coordinate concerns the height of vortices but it is irrelevant for the wavelength of azimuthal waves. The period of azimuthal waves shown in Fig. 5a is a function of number of waves, angular velocity of waves and drifting velocity of vortices. The amplitude of the velocity gradient components at different position z is given by the envelope of the oscillations which is not shown. The meaning of different symbols is also shown in this figure. The notion of filtered velocity gradient is introduced. This means velocity gradient or its components where the azimuthal waves were filtred out by a Butterworth filter, see $\gamma_{\theta f}$ and γ_{zf} in Fig. 5a. The course of filtered wall velocity gradients and their components is similar to the wall velocity gradients in Taylor-Couette non wavy flow (Sobolik et al, 2011).

From the point of view of the axial velocity, the outflow creates a forward critical point on the outer cylinder, see Fig. 5a. The azimuthal component of velocity gradient exhibits a maximum at this point and a minimum at the rear critical point (inflow). The axial component of velocity gradient is zero at these points. In fact, there is a small finite value of axial velocity gradient due to the drifting velocity of vortices. The amplitude of azimuthal waves, given by the envelope of oscillations, has azimuthal a_θ, and axial component a_z. The azimuthal component is zero in forward and rear critical points. The axial component has a maximum in forward critical point and it is very small at the extremes of γ_{zf}. Like in the classical forward critical point, the amplitude of axial oscillations, a_z, exhibits maxima and the variation of γ_{zf} is steep and almost linear. It is much steeper than in the inflow. The outflow has the form of a narrow jet with a high radial and azimuthal velocity.

Even if the amplitude of the axial component of velocity gradient has its maximum at the forward critical point, the oscillations of absolute value velocity gradient are very small, see Fig. 5b. It is due to the high value of azimuthal velocity gradient which is steady at this point.

We observed the transition from Taylor vortex flow into wavy vortex flow at Ta= 80.5. This value is much higher than the values calculated by Jones 1985. From his Fig. 3, we deducted values of 55.0, 57.6 and 64.5 for set-up of 1, 2 and 3 waves, respectively. We found always three waves at the transition which is in agreement with the simulations carried out by Jones.

The components of wall velocity gradient measured at different rotational rate are shown in Figs 6, 7 and 8. The rate of data acquisition was equal to 40 1/s. At the lowest rotational rate, Ta=97 (Fig. 6), the regime of three azimuthal waves was stable. The amplitude of wall shear rate and its azimuthal component was almost zero at the critical points. The amplitude of axial component exhibited maximum at the forward critical point and a small value at the rear critical point. Minima of the axial amplitude are located at the crest of $\gamma_{\theta f}$. At these points, the azimuthal amplitude exhibited maxima. This scenario did not change with increasing rotational rate. The only exception was that the axial amplitude had an almost constant value in the outflow region. The characteristic values of the vortices are shown in Table 1.

Ta	n	A_z	a_z	a_θ	$\gamma_{\theta max}$	$h.10^3$
97	3	4.8	4.1	2.4	13.7	11.2
202	4	21.1	14.3	7.5	46.3	11.1
483	2	60.4	74.4	52.9	194	11.1

Tab. 1: Parameters of wavy vortex flow shown in Figs 6 -8.

The axial component of the wall shear rate can be compared to the wall shear rate in classical impinging jet even if the azimuthal component in the forward stagnation point exhibits a maximum. According to Prandtl's boundary theory (Schlichting 1968), it holds for the stagnation region of an impinging jet that the wall shear rate is proportional to the distance from the stagnation point. The maximum of the wall shear rate is at the transition from the stagnation zone to the wall jet region. The spatial distribution of the wall shear rate fluctuations depends on the jet Reylnolds number and the distance of the orifice from the plate (Alekseenko and Markowich 1994). It can have a maximum or minimum in the stagnation point or a constant value in the jet region. At Ta=97, the amplitude of γ_z had maximum at the forward stagnation point and with increasing Ta the amplitude became almost constant in the outflow zone. Jones (1985) concluded that the strong azimuthal jets at the outflow region destabilize the flow making the vortices wavy. Coughlin and Marcus (1992) supposed that the both radial and azimuthal jets and axial gradient of the azimuthal velocity are responsible for the waviness. The strong azimuthal jet manifests itself by the maxima of $\gamma_{\theta f}$ in Figs 6-8. It increases with the Taylor number. The strength of radial jet can be deduced from the axial gradient of γ_{zf}. Its maximum value is also in the forward critical point.

Akonur and Lueptow (2003) estimated the mean value of the azimuthal shear stress from the PIV measurements for a radius ratio of 0.81. The values were normalized by the shear stress at transition to the Taylor vortex flow $\tau_{r\theta} / \tau_{r\theta,tr}$. As the shear stress is a linear function of velocity gradient with viscosity as a multiplication constant, these values can be compared with our values of $\gamma_\theta / \gamma_{\theta,tr}$, see Table 2. Our values are about 40 % higher than that of Akonur and Lueptow. This is caused by the inability of PIV to measure close enough to a wall. Due to this fact, the data on shear stress of Akonur and Lueptow exhibit a discontinuity close to the walls.

Akonur and Lueptow		**This work**	
Ta	$\tau_{r\theta} / \tau_{r\theta tr}$	Ta	$\gamma_\theta / \gamma_{\theta tr}$
117	4.5	121	6.3
286	15	284	21.4

Tab. 2: Comparison of normalize mean values of wall shear stress and velocity gradient.

The velocity gradients and their components were

calculated from the measured limiting diffusion currents using the quasi-steady approach, i.e. the Lévêque solution. Taking into account the inertia of the

diffusion boundary layer, the amplitudes of oscillations will be even higher.

IV. Conclusions

The three-segment ellectrodiffusion probes are convenient for the mapping of the velocity gradient components on the wall of the wavy Taylor-Couette-Poiseuille flow.
The form of the axial distribution of filtered wall shear rate components is similar to the distribution in steady Taylor vortices. However, the maximal values are more important.
Jet like outflow characterised by forward critical point was identified. The oscillations of axial component of velocity gradient exhibit maximum oscillations whereas the oscillations of the azimuthal component are negligible in the forward critical point.
The effect of the inertia of the boundary layer on the oscillation amplitudes should be studied in the future.

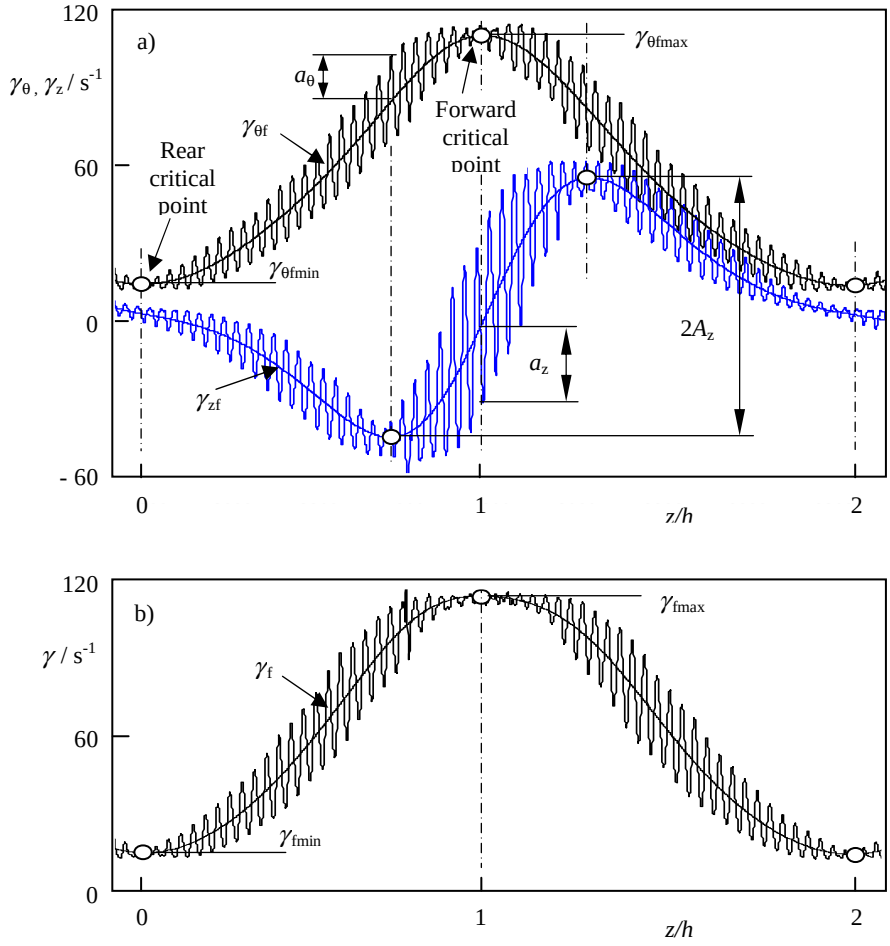

Fig. 5 : Characteristic values of velocity gradient (b) at its components (a) at *Ta* = 323, *h*= 12 mm.

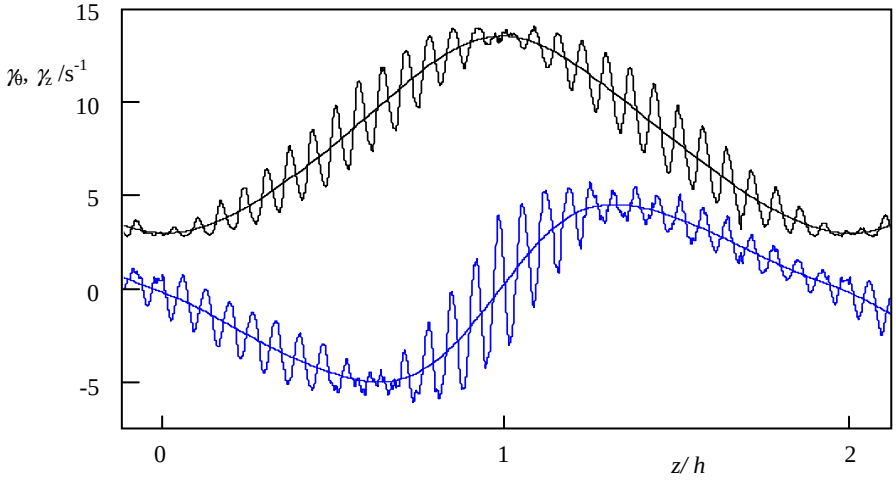

Fig. 6: Components of velocity gradient at *Ta*=97, *h* =11.2 mm.

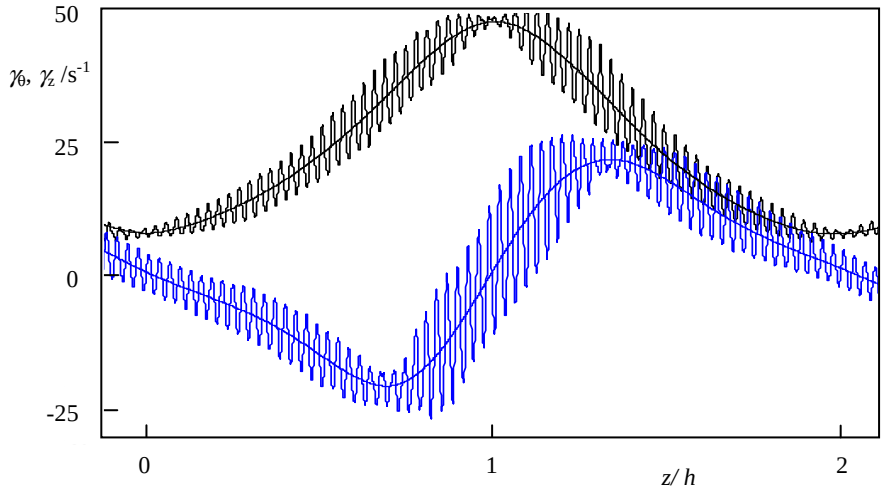

Fig. 7: Components of velocity gradient at *Ta* =202, *h* =11.1 mm.

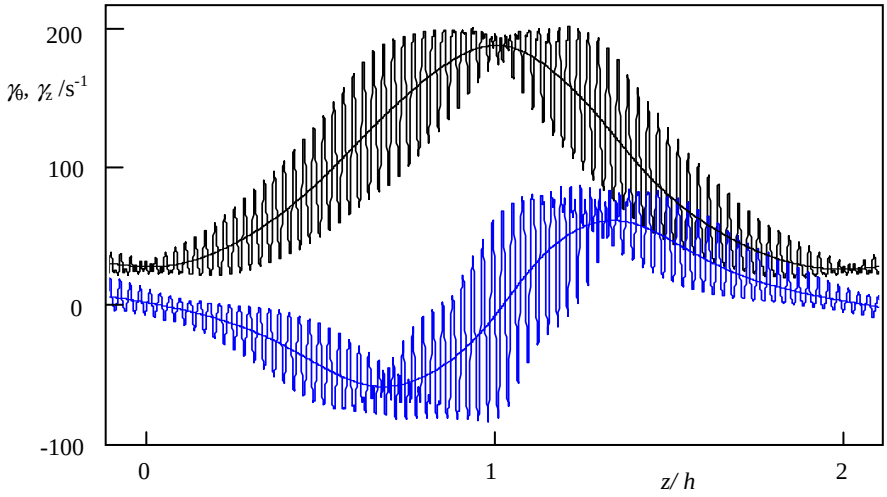

Fig. 8: Components of velocity gradient at *Ta* =483, *h* =11.1 mm.

Acknowledgements

This work was supported by the “Agence National de la Recherche”, France, by the grant number ANR-08-BLAN-0184-01.

References

Akonur A., Lueptow R.M., *Three-dimensional velocity field for wavy Taylor-Couette flow*, Physics of Fluids, 15, 947-960 (2003).

Alekseenko S., Markovich D.M., *Electrodiffusion diagnostics of wall shear stresses in impinging jets*, Journal of Applied Electrochemistry, 24, 626-631 (1994).

Cognet G., *Utilisation de la polarographie pour l’étude de l’écoulement de Couette*. Journal de Mécanique 10, 65-90 (1971).

Coughlin K.T., Marcus P.S., *Modulated waves in Taylor-Couette flow Part 2. Numerical simulation*, Journal of Fluid Mechanics, 234, 19-46 (1992).

Gogoi N.C., Dutta N.N., *Empirical approach to solid-liquid mass transfer in a three-phase sparged reactor*. Fuel Processing Technology, 48, 145-157 (1996).

Gruber R., Melin T., *Mixed convection in the copper dissolution technique of studying mass transfer*. International Journal of Heat and Mass Transfer, 46, 2403-2413 (2003).

Jones C.A., *The transition to wavy Taylor vortices*, Journal of Fluid Mechanics, 157, 135-162 (1985).

Kuhnel W., Kottke V., *Visualization and determination of local mass transfer at solid walls in liquid flow*, Revue Générale de Thermique, 37, 256-265 (1998).

Lebouché M., *Relation entre les fluctuations pariétales du transfert massique et du gradient de vitesse dans le cas d’un nombre de Schmidt grand*, Comptes Rendus de l’Académique des Sciences, 271, 438-441 (1970).

Lévêque M.A., *Les lois de la transmission de la chaleur par convection*, Ann. Mines, 13, 201-239 (1928).

Raguin L.G., Shannon M., Georgiadis L.G., *Dispersion radiale et axiale dans les écoulements tourbillonnaires de Taylor-Couette et Poiseuille.* International Journal of Heat and Mass Transfer, 44, 3295-3306 (2001).

Schlichting, H., *Boundary Layer Theory*. McGraw-Hill, New York, (1968).

Sobolik V., Mitschka P., Menzel T., *Method of manufacture of segmented probe with circular cross-section*. Czech Patent. N° 262 823 (1988).

Wein O., Sobolik V., *Theory of direction sensitive probes for electrodiffusion measurement of wall velocity gradients*. Collection Czechoslovak Chemical Communications, 52, 2169 - 2180 (1987).

Sobolik V., Jirout T., Havlica J., *Wall shear rates in Taylor vortex flow.* Journal of Applied Fluid Mechanics, 4, 25-31

(2011).